metals

MDPI

Article

# Analysis of Fatigue and Wear Behaviour in Ultrafine Grained Connecting Rods

**Rodrigo Luri, Carmelo J. Luis, Javier León, Juan P. Fuertes, Daniel Salcedo and Ignacio Puertas ***

Mechanical, Energetics and Materials Engineering Department, Public University of Navarre, Campus Arrosadía s/n, Pamplona 31006, Spain; rodrigo.luri@unavarra.es (R.L.); cluis.perez@unavarra.es (C.J.L.); javier.leon@unavarra.es (J.L.); juanpablo.fuertes@unavarra.es (J.P.F.); daniel.salcedo@unavarra.es (D.S.)

* Correspondence: inaki.puerta@unavarra.es; Tel.: +34-948-169-305

Received: 3 July 2017; Accepted: 20 July 2017; Published: 29 July 2017

**Abstract:** Over the last few years there has been an increasing interest in the study and development of processes that make it possible to obtain ultra-fine grained materials. Although there exists a large number of published works related to the improvement of the mechanical properties in these materials, there are only a few studies that analyse their in-service behaviour (fatigue and wear). In order to bridge the gap, in this present work, the fatigue and wear results obtained for connecting rods manufactured by using two different aluminium alloys (AA5754 and AA5083) previously deformed by severe plastic deformation (SPD), using Equal Channel Angular Pressing (ECAP), in order to obtain the ultrafine grain size in the processed materials are shown. For both aluminium alloys, two initial states were studied: annealed and ECAPed. The connecting rods were manufactured from the previously processed materials by using isothermal forging. Fatigue and wear experiments were carried out in order to characterize the in-service behaviour of the components. A comparative study of the results was made for both initial states of the materials. Furthermore, Finite Element Modelling (FEM) simulations were used in order to compare experimental results with those obtained from simulations. In addition, dimensional wear coefficients were found for each of the aluminium alloys and initial deformation states. This research work aims to progress the knowledge of the behaviour of components manufactured from ultrafine grain materials.

**Keywords:** fatigue; wear; ECAP; FEM

## 1. Introduction

Over the last few years there has been a large number of scientific research works dealing with Equal Channel Angular Pressing (ECAP) and other Severe Plastic Deformation (SPD) processes that have arisen after ECAP was first proposed by Segal et al. [1]. Initially, these works dealt mainly with improvement in the mechanical properties of the so-processed materials, as can be observed in [2–5], as well as with the analysis of the final microstructure [6]. Some other research works dealt with the analysis of different processing routes [7] as well as with the proposal of new SPD processes, such as ECAP-Conform [8], Repetitive Corrugation and Straightening (RCS) [9], Accumulative Roll-Bonding (ARB) [10], and High-Pressure Torsion (HPT) [11], among many others. However, the number of scientific works dealing with fatigue and wear analysis is much lower.

Nowadays there is a tendency to develop mechanical components from previously SPD processed materials and hence to scale the ECAP process in order to be able to obtain higher dimensions in the ECAPed parts with the aim of obtaining mechanical components with possible industrial applications. As can be observed in [12], the ECAP process is employed for processing billets with 15 mm × 15 mm × 120 mm and 50 mm × 50 mm × 900 mm in order to compare the results obtained. Among the results obtained by these authors it should be mentioned that the required pressure to carry out the process is linearly increased as a consequence of the contact surface which is also increased [12].

These authors have also found that there are no significant differences between the homogeneity of the hardness properties and the microstructure obtained [12]. On the other hand, Horita et al. [13] analysed cylindrical billets with different initial diameters (6 and 40 mm). They found that the ultrafine grain size and the mechanical properties obtained are independent of the initial size of the billets [13].

Other studies which try to obtain industrial applications of SPD billets are those related to manufacturing of mechanical components. Among these studies the development of: medical implants [14], gears [15], and blades [16] should be mentioned. Most of the mechanical components manufactured after these SPD processes are developed by using subsequent thermomechanical processes such as forging or isothermal forging [15,16], among others. This allows for an analysis of the improvement in the mechanical properties and in the microstructure of functional parts which is much closer to the actual working conditions than the measure of properties in the billets after the SPD processes.

Among the mechanical properties to be studied in the SPD processed materials, fatigue and wear behaviour should be mentioned. Some studies dealing with the fatigue test have led to the conclusion that at room temperature the previously SPD processed materials are able to withstand a lower number of fatigue cycles than those which have not been previously processed by ECAP [17] as a consequence of the high amount of dislocation that exists inside the so-processed materials. When the ECAP process is carried out by increasing the processing temperature it is possible to obtain an improvement in the fatigue life in the ultrafine grained materials [18]. In this way, Goto et al. [19] analysed the influence of the number of ECAP passages in the fatigue behaviour of a copper alloy after 4, 8, and 12 passages. Gröber et al. [20] analysed the fatigue behaviour of bolts both with ultrafine grain size after ECAP and without ultrafine grain size. In the bolts manufactured after ECAP they obtained a reduction in the number of cycles before failure between 28% and 68% depending on the applied load [20].

In the studies dealing with wear behaviour, it has been found that lower wear is obtained in the materials previously processed by ECAP than that obtained in the non-processed materials. As these previously ECAPed processed parts have a lower value of wear, a lower loss of volume [21–24] is obtained in the parts. In addition, a great deal of attention has been paid to the wear resistance of copper [25–27] and copper alloys [28] processed by severe plastic deformation processes.

In [21–23] ECAP is employed as a method to obtain ultrafine grain size in the billets while in [24] the SPD process known as High-Pressure Torsion (HPT) is employed. Moreover, the method mainly employed to analyse the wear in these parts is ball-on-disk [21,22,24]. Some other authors employed the method known as block-on-disk [23] to analyse the wear behaviour in SPD billets. However, the number of scientific works that analyse the wear behaviour in functional parts is scant. In order to bridge the gap, in this present research work, an analysis of the wear obtained in connecting rods manufactured by ECAP is carried out. As will be shown later, these mechanical parts were obtained by using route C and after isothermal forging. Previously, fatigue tests were carried out in order to determine the fatigue life of these mechanical parts and then wear tests were carried out on equipment, which had been specifically developed to analyse the behaviour of these components. Results are compared with those obtained in non-ECAPed processed parts. In addition, dimensional wear coefficients were found for each of the aluminium alloys and initial deformation states. Also, a comparison between Finite Element Modelling (FEM) and experimental results was carried out.

## 2. Set-Up of the Experimentation

In order to carry out the present study, connecting rods, made of AA5083 and AA5754, were manufactured by isothermal forging. Two initial states were considered for the alloys which correspond with annealed material and material previously processed by the severe plastic deformation process known as Equal Channel Angular Pressing (ECAP). Figure 1 shows the phases involved in the manufacturing of the connecting rods.

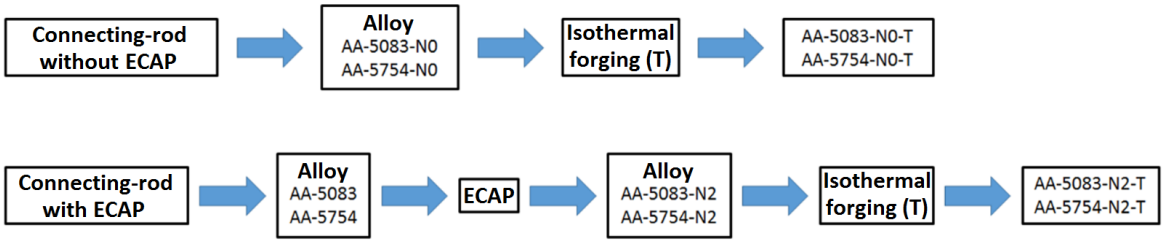


**Figure 1.** Phases in the manufacturing of the connecting rod; ECAP: Equal Channel Angular Pressing.

The ECAPed material was processed by using a press with a set of ECAP dies with a channel diameter of 20 mm and an intersection angle between the two channels of 90°. Moreover, the fillet radii between the channels had the same values, equal to 2.5 mm. Then the material was isothermally forged to obtain the connecting rods. The non ECAPed material was obtained after an annealing heat treatment and then isothermally forged. In the case of the ECAPed material, the connecting rods made of AA5083 were isothermally forged at 200 °C, while those made of AA-5754 were isothermally forged at 150 °C

In order to carry out the wear test in the connecting rods it is necessary to determine the working conditions of these mechanical components. As is well-known, when the connecting rods form part of a mechanism, they should function below the threshold given by the yield stress limit so that they have an infinite fatigue limit. That is to say, failure will never occur except in the case that some manufacturing defects exist inside the mechanical components. In this way, the useful working life of the component is determined by the wear behaviour of the movable contact surfaces.

With the aim of determining the fatigue limit it is necessary to obtain the working loads and these should accomplish two constraints. The first deals with the values of the applied loads which should be below the fatigue limit of the component and the second deals with the contact pressure which should be below the yield stress of the material.

Therefore, before carrying out the wear analysis, it is necessary to carry out mechanical test and fatigue simulation to determine both the fatigue limit of the component as well as the contact pressures. With this aim, both FEM simulations and the experimental fatigue test were carried out to determine the working ranges of the manufactured parts.

In order to carry out the experimental fatigue test, zero crossing was avoided, meaning that the component was subjected to an average stress and a variable stress so that the load was always positive where the minimum force was close to zero.

### *2.1. Finite Element Modelling (FEM) Simulations*

For the forging process of the preform, a similar geometry to that used in [29] was selected. In order to simulate the manufacturing of this connecting rod by the finite element method, the process was divided into two different strokes. The contact simulated between the three bodies is of node-to-segment type and the friction coefficient selected is of shear type with a value of 0.3. The preform meshing consists of Overlay-Hex type elements (with eight integration nodes) whose maximum and minimum size values are 0.6 mm and 0.25 mm, respectively. Furthermore, a coarsening factor of 2 is selected and these parameters are held constant in the subsequent re-meshing processes. A multifrontal-sparse solver is employed. This first stroke is simulated by using SimufactForming™ (MSC Software, Newport Beach, CA, USA). The preform of the connecting rod is isothermally forged at a temperature of 200 °C and the material used in the FEM simulations is a 5083 aluminium alloy in a predeformed state through two ECAP passages with route C (N2). The flow rule proposed by [30] is assigned to the material in order to consider this predeformed state of the AA5083. This flow stress is shown in Equation (1), whose main parameters are defined in [30].

$$\sigma_N = \sigma_2 + \left(a + \frac{b \times \varepsilon^n}{c + \varepsilon^2}\right) \times e^{-d \times \varepsilon} \quad (1)$$

Figure 2a,b show that the highest damage value takes place at the outer zone of the top with a value of 0.271.

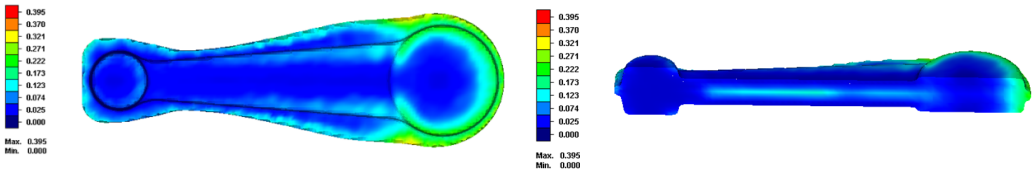


(**a**) (**b**)

**Figure 2.** Distribution of strain and damage values during the first forging stroke: (**a**) Damage values and (**b**) damage values at longitudinal section.

In order to model the second and final forging stroke, contact and temperature conditions, as well as the assigned flow rule for the material, are the same as those for the first stroke. Figure 3a,b show that the zone where the highest value is achieved, according to Crockroft-Latham's criterion, is located at the surface of the top with values of around 0.3. Therefore, it can be concluded that no cracks will appear in the connecting rod made of AA5083 predeformed by ECAP when this is forged with two strokes at a temperature value of 200 °C.

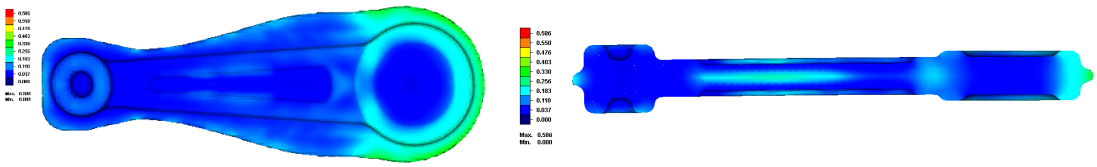

(**a**) (**b**)

**Figure 3.** Distribution of strain and damage values during the second forging stroke: (**a**) Damage values and (**b**) damage values at longitudinal section.

Therefore, taking the study carried out by [31] into account, no cracks will occur either during the first or the second forging stroke. Figure 4 shows the set of dies employed in the manufacturing of the connecting rods that were tested in this present research work.

**Figure 4.** Set of dies used in the manufacturing of the connecting rods.

Moreover, FEM simulations were performed by considering tension loads using MSC. Marc™ (MSC Software, Newport Beach, CA, USA). From these results, the stresses to which the connecting rod

is being subjected in each considered case were obtained. This data is used along with the experimental fatigue test to determine both the average and variable loads as well as to determine the useful life of the connecting rod under these working conditions. The geometry of the manufactured connecting rod is shown in Figure 5.

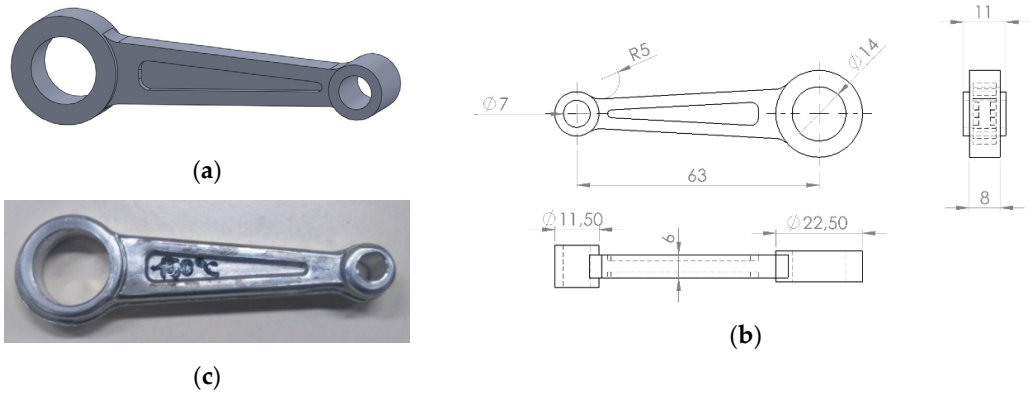


**Figure 5.** (**a**) CAD Design; (**b**) dimensions of the connecting rod; (**c**) connecting rod manufactured.

The meshing of the solid geometry is shown in Figure 6. This meshing is smaller at the bottom, top, and fillet radii of the connecting rod.

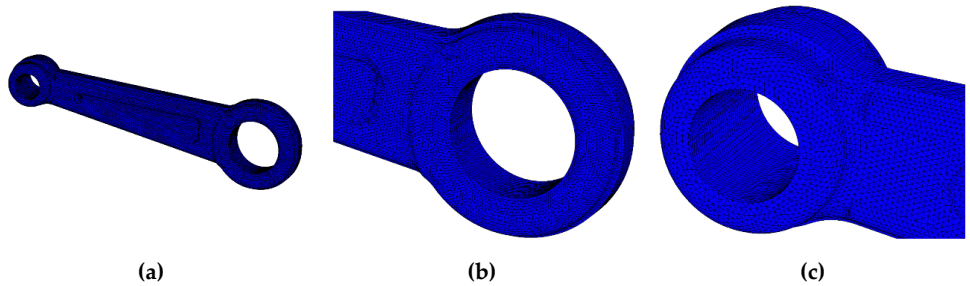


**Figure 6.** (**a**) Meshing of the connecting rod; (**b**) and (**c**) detail of the meshing at the top and at the bottom of the connecting rod.

A rigid contact is employed for both the bottom and the top of the connecting rod. Both rigid contacts are modelled by two cylinders that simulate the pin joints placed at the bottom and at the top of the connecting rod. The contact shown in Figure 7c has a non-displacement constraint. On the other hand, in the contact shown by Figure 7b a tension load is applied which is transmitted to the connecting rod.

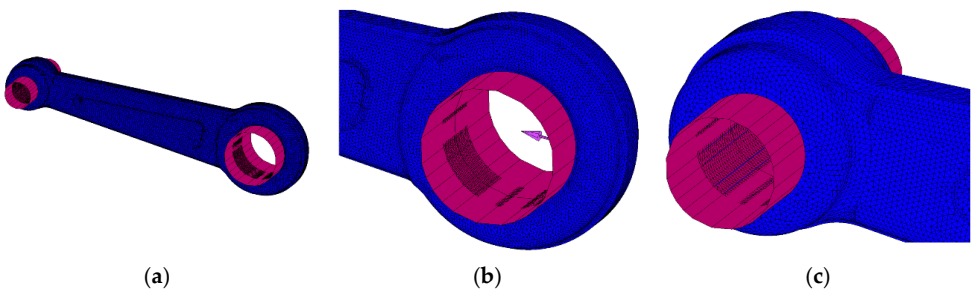


**Figure 7.** (**a**) Contacts and applied load; (**b**) and (**c**) detail of the boundary conditions at the top and at the bottom of the connecting rod.

AA5754 and AA5083 aluminium alloys were selected both with a Young modulus of 70 GPa and a Poisson coefficient equal to 0.3. As can be observed in Figure 7, the load applied at the top of the connecting rod is equal to 1 kN. Figure 8 shows the Von Mises stress when this load of 1 kN was applied.

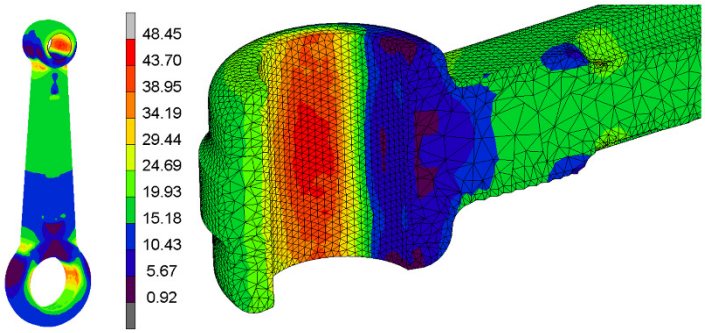


**Figure 8.** Equivalent Von Mises Stress (MPa) when the applied load is equal to 1 kN.

As can be observed, the maximum value of the equivalent Von Mises stress is achieved at the bottom of the connecting rod, specifically in the inner surface which is in contact with the pin joint. Equation (2) shows the stress tensor in this zone as a function of the applied tension load.

$$\sigma_{\text{tension}} = \text{Load}_t \begin{pmatrix} 53.84 & -13.74 & 0.92 \\ -13.74 & 3.89 & 0.89 \\ 0.92 & 0.89 & 17.32 \end{pmatrix} \text{(MPa)} \quad (2)$$

The experimental fatigue tests were carried out in pure tension loads, with the minimum stress being equal to zero. This means that an average stress ($\sigma_m$) and a variable stress ($\sigma_a$) exist. From these stresses it is possible to determine the equivalent average stress ($\sigma_{\text{tension\_aeq}}$). In order to determine the stress tensors it is necessary to know the behaviour of the applied loads in advance with the aim of determining both the maximum and the minimum stresses. From these values, it is then possible to determine both the average stress and the variable stress as Equations (3) and (4) show, respectively.

$$\sigma_m = \frac{\sigma_{max} + \sigma_{min}}{2} \quad (3)$$

$$\sigma_a = \frac{\sigma_{max} - \sigma_{min}}{2} \quad (4)$$

In order to carry out the fatigue test a maximum load was set up ($F_{max}$), with the minimum load $F_{min}$ being equal to zero. From these values, it is possible to determine the stress tensors, as Equations (5) and (6) show.

$$\sigma_{\text{tension\_max}} = F_{max} \begin{pmatrix} 53.84 & -13.74 & 0.92 \\ -13.74 & 3.89 & 0.89 \\ 0.92 & 0.89 & 17.32 \end{pmatrix} \text{(MPa)} \quad (5)$$

$$\sigma_{\text{tension\_min}} = 0 \quad (6)$$

By substitution of Equations (5) and (6) into Equations (2) and (3), Equation (7) is attained which allows us to obtain both the average and the variable tensions that are being applied to the connecting rod.

$$\sigma_{\text{tension\_m}} = \sigma_{\text{tension\_a}} = \frac{F_{max}}{2} \begin{pmatrix} 53.84 & -13.74 & 0.92 \\ -13.74 & 3.89 & 0.89 \\ 0.92 & 0.89 & 17.32 \end{pmatrix} \text{(MPa)} \quad (7)$$

By diagonalization of the stress tensors shown by Equation (7), it is possible to obtain the stress tensors shown by Equation (8).

$$\sigma_{tension\_m} = \sigma_{tension\_a} = \frac{F_{max}}{2}\begin{pmatrix} 57.38 & 0 & 0 \\ 0 & 17.38 & 0 \\ 0 & 0 & 0.29 \end{pmatrix} (MPa) \quad (8)$$

As can be found in [32] and [33], in order to determine the equivalent variable stress ($\sigma_{tension\_aeq}$) it is necessary to apply the Von Mises Criterion to the tensor given by ($\sigma_{tension\_a}$). Moreover, in order to determine the average equivalent stress ($\sigma_{tension\_meq}$) it is also necessary to apply the Von Mises criterion to the tensor ($\sigma_{tension\_m}$), where a positive sign is to be used if the trace of the diagonal tensor is positive and a negative one if this trace is negative. Then Equation (9) may be obtained [32] and [33].

$$\sigma_{tension\_aeq} = \sigma_{tension\_meq} = 71.77\left(\frac{F_{max}}{2}\right) (MPa) \quad (9)$$

As can be observed in [32] and [33], with both the equivalent average stress ($\sigma_{meq}$) and the equivalent variable stress ($\sigma_{aeq}$) it is possible to determine the equivalent fatigue stress ($\sigma_{Nf}$). This equivalent fatigue stress is a variable stress which is equivalent to the cycle with average stress equivalent ($\sigma_{meq}$) and variable stress equivalent ($\sigma_{aeq}$). Equation (10) allows us to obtain ($\sigma_{Nf}$) where ($\sigma_{UTS}$) the ultimate tension stress of the material is that being analysed.

$$\sigma_{Nf} = \frac{\sigma_{UTS}}{\sigma_{UTS} - \sigma_{meq}}\sigma_{aeq} (MPa) \quad (10)$$

By replacing Equation (10) into Equation (9), it is possible to obtain Equation (11).

$$\sigma_{tension\_Nf} = \frac{35.89\ \sigma_{UTS}\ F_{max}}{\sigma_{UTS} - 35.89\ F_{max}} (MPa) \quad (11)$$

From the above-mentioned procedure it is possible to determine the equivalent fatigue stress which is being applied to the connecting rods when the experimental fatigue tests are being carried out under different loads.

### *2.2. Experimental Analysis*

As was previously mentioned, the connecting rods were isothermally forged at different temperatures depending on the alloy. That is, the connecting rods made of AA5083 were isothermally forged at 200 °C, while those made of AA-5754 were isothermally forged at 150 °C. These so-manufactured parts were named as: AA-5083-N2-T200 and AA-5754-N2-T150, where N2 refers to the initial state after two ECAP passages. The experimental fatigue tests were carried out on the connecting rods under different loads. These applied loads, as well as the number of cycles that they have withstood, are shown on Table 1. Given the variability that exists in the fatigue test, for each alloy and initial state, the test was repeated for the mean load of the considered interval.

**Table 1.** Number of cycles withstood by the connecting rods in the fatigue test under different loads.

| Connecting Rod | $F_{max}$ (kN) | $F_{min}$ (kN) | Number of Cycles |
|---|---|---|---|
| AA-5083-N2-T200 | 3 | 0 | 167,193 |
| | 4 | 0 | 63,805 |
| | 4 | 0 | 69,696 |
| | 5 | 0 | 26,299 |
| AA-5754-N2-T150 | 2 | 0 | 575,581 |
| | 3 | 0 | 215,185 |
| | 3 | 0 | 219,493 |
| | 4 | 0 | 85,898 |

Figure 9 shows four of the tested connecting rods after failure by fatigue. It should be mentioned that in all the connecting rods tested, the failure was observed at the bottom, as was expected.

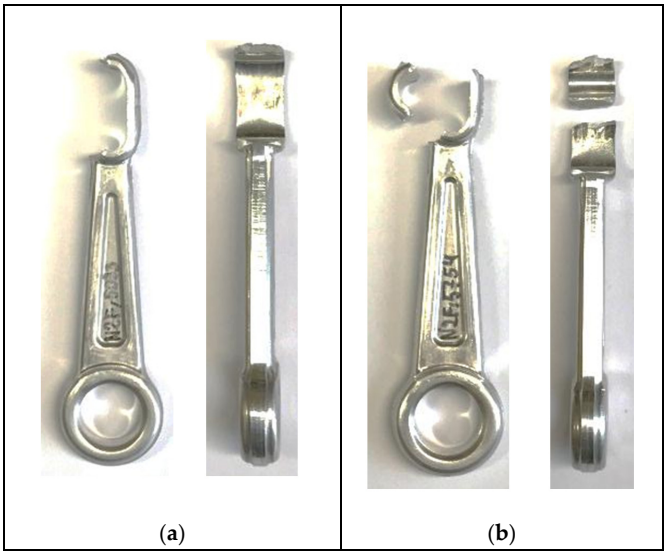

**Figure 9.** Connecting rods after fatigue breakage: (**a**) AA-5083-N2-T200, $F_{max}$ = 4 kN, 69,696 cycles; (**b**) AA-5754-N2-T150, $F_{max}$ = 3 kN, 219,493 cycles.

In Figure 10a the influence of the applied load over the number of cycles that is capable of withstanding the connecting rod can be observed. By taking into consideration that the ultimate tension stresses of the aluminium alloys: AA5754-N2-T150, and 5083-N2-T200 are 312 and 485 MPa, respectively, and by using Equation (11), it is possible to obtain Figure 10b which shows both the average equivalent stress and the number of cycles that the connecting rods are capable of withstanding at this equivalent stress.

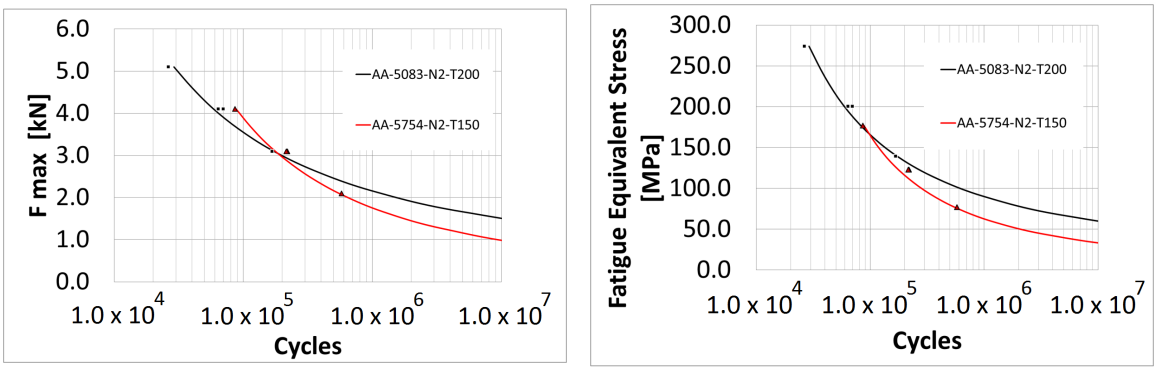


(**a**) (**b**)

**Figure 10.** Fatigue diagrams: (**a**) Maximum load vs number of cycles; (**b**) equivalent variable stress vs number of cycles.

If we assume that $1.0 \times 10^7$ cycles is equivalent to the endurance life of the connecting rods then from Figure 10 it is possible to affirm that the manufactured connecting rods will withstand more than $1.0 \times 10^7$ cycles if the maximum applied load is below 1 kN. This value is considered as a maximum value to apply to the connecting rods in the wear tests which are shown in the following sections.

## 3. Analysis of the In-Service Behaviour of the Manufactured Connecting Rod

In this section an analysis of the wear that the manufactured parts undergo is made. In addition, a comparison between both experimental and FEM results is carried out.

### *3.1. In-Service Analysis of the Wear*

In order to perform the experimental wear tests in the isothermally forged connecting rods, the equipment shown in Figure 11 was employed which was specifically designed for this purpose.

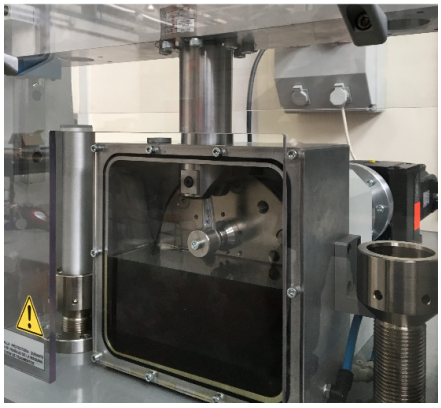

**Figure 11.** Testing machine of connecting rods.

The equipment shown in Figure 11 is similar to a crank and connecting rod mechanism where the disk represents the crank. It is composed of a disk which is fixed to a servomotor, where the top of the connecting rod is linked, and with a crossbar that is capable of sliding between a pair of columns so acting as a piston, which is linked to the bottom of the connecting rod. Over this crossbar a spring acts so that the connecting rod undergoes compressive loads as the disk rotates. As may be observed, a lubricant was used in the experiment (synthetic oil 5W30).

When the connecting rod is placed at the bottom dead centre it is possible to preload the spring. In the tests carried out a preload of 0.2 kN was used to avoid possible clearances in the tests. As the length of the crank is 20 mm, then the piston stroke is 40 mm, where this length is the compression length of the spring. The springs used in the experiments have a spring constant of 20 N/mm. From Equation (12) it is possible to determine that the maximum load which undergoes the connecting rod is equal to 1 kN, being the minimum load, the applied preload.

$$F_{\max} = F_{\text{preload}} + k\Delta x \ (\text{N}) \tag{12}$$

As was previously mentioned in Section 2, in the current tests, the connecting rods will have an endurance life (withstanding more than $10^7$ cycles) if the value of the maximum load is equal to 1 kN. Then if failure exists before this limit, it will be mainly attributed to wear phenomena. In all the performed tests the rotating speed was 60 rpm.

Connecting rods were made of AA5083 and AA5754 both from materials having ultrafine grain size and from annealed materials. As was previously mentioned, in the ECAPed materials, AA5083 connecting rods were isothermally forged at 200 °C (AA-5083-N2-T200) and AA5754 connecting rods were isothermally forged at 150 °C (AA-5754-N2-T150).

In order to compare the properties of the connecting rods manufactured from ultrafine grained material with those of the connecting rods that were manufactured from annealed material, these latter parts were isothermally forged following recommendations of [34], where a temperature of 380 °C is suggested for forging the two aluminium alloys. Therefore, 380 °C was used as forging temperature for the connecting rods made of previously annealed aluminium alloys which were

named as (AA-5083-N0-T380 y AA-5754-N0-T380). Next the so-manufactured connecting rods were tested up to $5 \times 10^4$ cycles and $1.5 \times 10^5$ cycles. Results obtained are shown in Table 2 and Figure 12. Figure 13 shows the wear at both the top and the bottom of the connecting rods after 150,000 cycles.

**Table 2.** Wear tests: Loss of volume ($V_{\text{initial}} - V_{\text{final}}$) (mm$^3$).

| Connecting Rod | ($V_{\text{init}} - V_{\text{final}}$) ($5 \times 10^4$ cycles) | ($V_{\text{init}} - V_{\text{final}}$) ($1.5 \times 10^5$ cycles) |
|---|---|---|
| AA-5083-N0-T380 | 12.6633 | 35.4100 |
| AA-5083-N2-T200 | 11.1991 | 31.6503 |
| AA-5754-N0-T380 | 7.8217 | 27.6833 |
| AA-5754-N2-T150 | 7.3636 | 25.6795 |

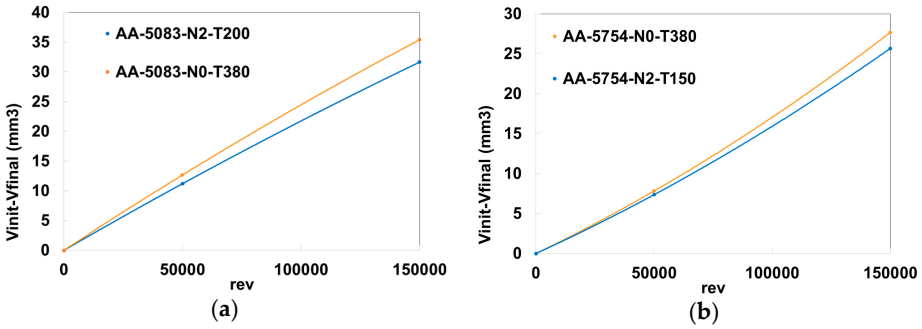


**Figure 12.** Wear vs number of revolutions: (**a**) AA-5083; (**b**) AA-5754.

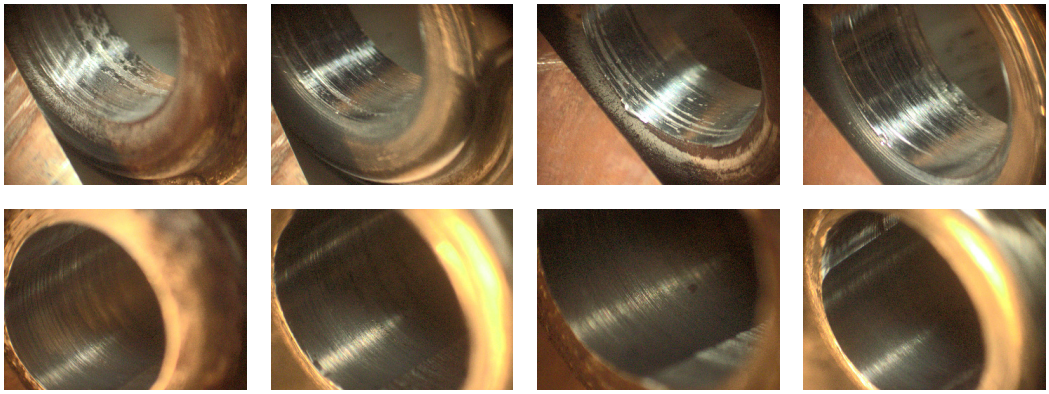


**Figure 13.** Wear in the connecting rods (upper figure = top of the connecting rod; lower figure = bottom of the connecting rod): (**a**) AA-5083-N0; (**b**) AA-5083-N2; (**c**) AA-5754-N0; (**d**) AA-5754-N2.

### *3.2. Simulation of the Wear by FEM*

From the FEM simulations it is possible to compare experimental results with those obtained from the simulation. In order to perform the simulations of the connecting rod a meshing as shown in Figure 5 was employed. A rigid-deformable contact was used where the deformable body corresponds to the connecting rod as well as to the cylindrical surfaces of the rigid bodies, as Figure 14 shows. In the pin joint with the higher diameter (cbody3) a rotation movement was imposed with a turning radius of 20 mm, because it is linked to the rotatory disk and it constitutes the crank of the mechanism.

In the pin joint with the lower radius (cobdy4) a constraint was imposed, which only allows displacement in the *Z*-direction. Moreover, it is linked to a spring with a constant of 20 N/mm which also has a preload of 0.2 kN, which corresponds with the experimental values. In this way the connecting rod makes a compressive load on the spring and so the load is increased up to 1 kN at the top dead centre, which corresponds with the experimental tests.

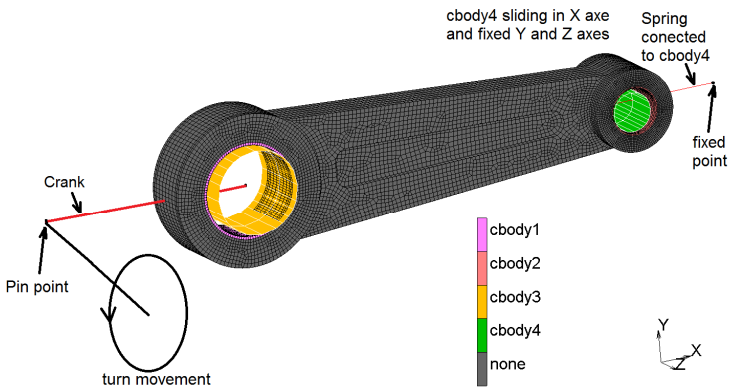


**Figure 14.** Connecting rod and pin joints.

Moreover, in the contacts employed in the simulation, the dimensional wear coefficient ($K$) was applied for each of the alloys shown in Table 3.

**Table 3.** Dimensional wear coefficients $K$ (M·Pa$^{-1}$).

| Connecting Rod | $K$ (M·Pa$^{-1}$) |
|---|---|
| AA-5083-N0-T380 | $8.317 \times 10^{-9}$ |
| AA-5083-N2-T200 | $7.434 \times 10^{-9}$ |
| AA-5754-N0-T380 | $6.556 \times 10^{-9}$ |
| AA-5754-N2-T150 | $6.082 \times 10^{-9}$ |

The maximum applied load is 1 kN, which corresponds with the endurance limit ($1.0 \times 10^7$ cycles), hence if a failure is observed, this may be mainly attributed to the wear undergone by the connecting rods over the contact surfaces. Figure 15 shows the wear index that the connecting rod, made of 5754-N2-T200, undergoes in one cycle (one revolution).

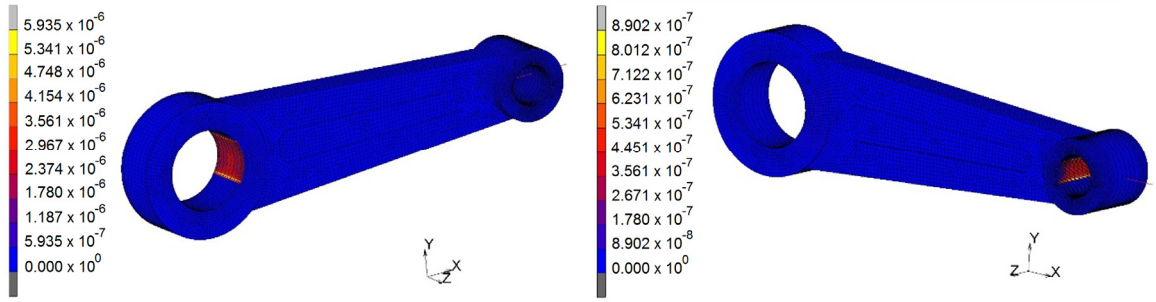


(**a**) (**b**)

**Figure 15.** Wear index 5754-N2-F: (**a**) Top; (**b**) bottom.

The highest wear is produced in the contact between the pin joint at the top of the connecting rod, which is approximately six times higher than that observed at the bottom of the connecting rod.

Simulations were also performed in the connecting rods made of AA-5083-N0-T380, AA-5083-N2-T200 and AA-5754-N0-T380 where the loss of volume was measured at $1.5 \times 10^5$ cycles, as shown in Table 4. Moreover, Table 4 shows the experimental loss of volume after $1.5 \times 10^5$ cycles, as well as the differences between both experimental and FEM results.

**Table 4.** Wear by loss in volume in both the Finite Element Modelling (FEM) and experimental results ($mm^3$) after $1.5 \times 10^5$ cycles.

| Connecting Rod | $(V_{init} - V_f)$ $(1.5 \times 10^5$ cycles) FEM | $(V_{init} - V_f)$ $(1.5 \times 10^5$ cycles) EXP | % Diff. |
|---|---|---|---|
| AA-5083-N0-T380 | 35.4089 | 35.4100 | 0.01% |
| AA-5083-N2-T200 | 31.3905 | 31.6503 | 0.82% |
| AA-5754-N0-T380 | 27.9116 | 27.6833 | 0.82% |
| AA-5754-N2-T150 | 25.8936 | 25.6795 | 0.83% |

As can be observed from Table 4, a good agreement exists between both experimental and FEM results.

### *3.3. Experimental Analysis of the Wear in the Connecting Rods*

As was previously-mentioned, the wear study for the connecting rods was made for two different aluminium alloys: AA5083 and AA5754. Once the connecting rods were manufactured, wear tests were carried out in a specifically designed equipment, which is shown in Figure 11.

The next step was to cut the connecting rods in such a way that they could be analysed by scanning electron microscopy (SEM) in order to study the different finishes of the surface. In order to do this, the selected zones to be studied were the inner zones of both the top and the bottom of the connecting rod. Figure 16 shows one of the cut connecting rods along with the zones to be studied.

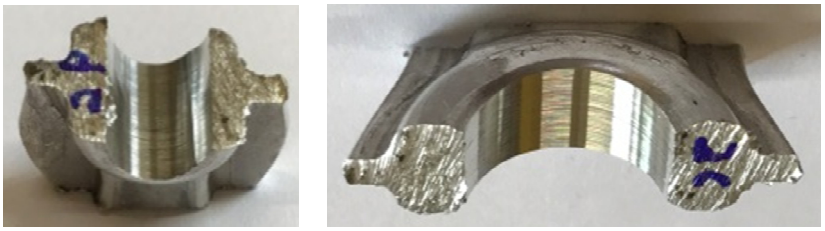

(**a**) (**b**)

**Figure 16.** Cut connecting rod and study zones: (**a**) Bottom of connecting rod; (**b**) top of connecting rod.

Previous to the SEM analysis, all the samples were cleaned with acetone in order to remove lubricant stains from the wear test. A scanning electron microscope JEOL 6400 (JEOL, Tokyo, Japan) was used and its most important working parameters are as follows: acceleration voltage of 20 kV and beam current of around 0.1 nA.

Figure 17 shows SEM micrographs for the AA-5083-N0-T380 connecting rod at three different magnifications: 50×, 200× and 1000× and at the top and at the bottom zones. At the top of the connecting rod and at magnifications of 50× and 200×, it can be observed that the grooves are homogeneously distributed. The differences observed in Figure 17 between the top and the bottom of the connecting rod may be attributed to the fact that there is a relative movement between the top pin joint and the top of the connecting rod, which is of one complete turn per cycle. There is another oscillating movement (of around 30°), thus causing the relative sliding between the pin joint and the bottom of the connecting rod to be much smaller. In spite of undergoing higher pressure values, because of a smaller contact area, the fact that the distance covered per cycle is lower leads to the higher wear values at the top of the connecting rod.

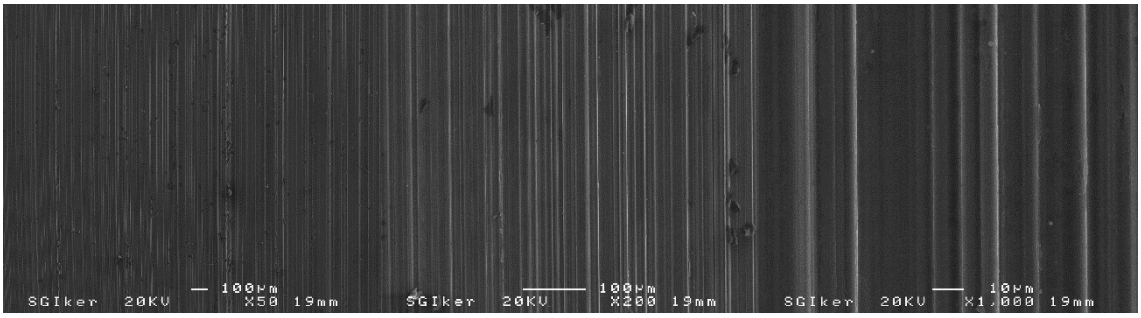


50× 200× 1000×

(**a**)

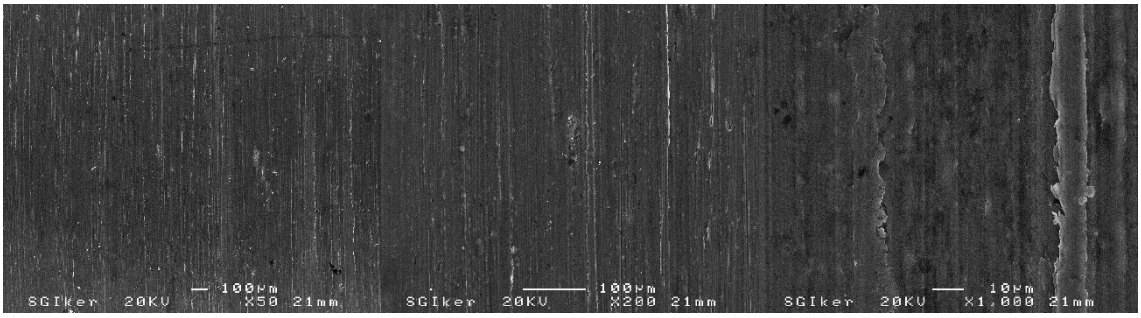


50× 200× 1000×

(**b**)

**Figure 17.** Scanning electron microscope (SEM) micrographs for AA-5083-N0-T380 connecting rod: (**a**) Top zone; (**b**) bottom zone.

Figure 18 shows the SEM micrographs for the AA5083-N2-T200 connecting rod. At the top zone, SEM micrographs are taken at three different magnifications: 50×, 200×, and 1000×, whereas at the bottom zone, these are taken at four different magnifications: 50×, 200×, 1000×, and 2500×. At the top zone, a very similar behaviour to that previously shown by the AA5083-N0-T380 connecting rod can be observed.

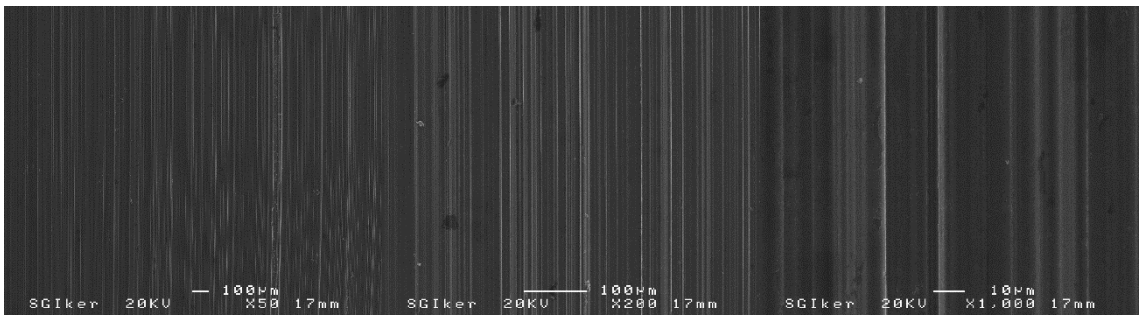


50× 200× 1000×

(**a**)

**Figure 18.** *Cont.*

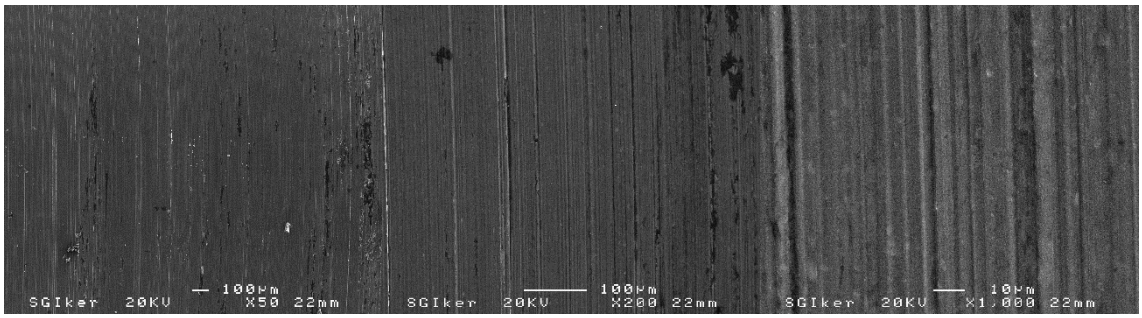


50× 200× 1000×

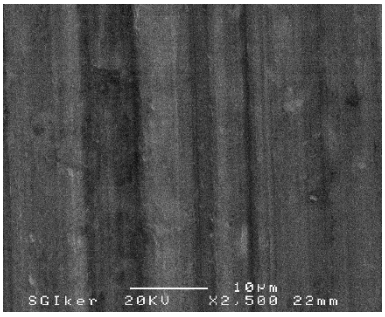


2500×

(**b**)

**Figure 18.** SEM micrographs for AA5083-N2-T200 connecting rod: (**a**) Top zone; (**b**) bottom zone.

Figure 19 shows SEM micrographs for the AA5754-N0-T380 connecting rod. At the top zone, images are taken at three different magnifications: 50×, 200×, and 1000×, and at the bottom zone, these are taken at two different magnifications: 200× and 1000×. At the top zone, it can be observed that there is a very similar behaviour to those obtained from AA5083 connecting rods, where grooves are completely aligned and with a similar width.

Finally, Figure 20 shows the SEM micrographs for the AA5754-N2-T150 connecting rod. The results obtained are equal to those observed in the case of AA5754-N0-T380. The fact that there are no significant differences between both starting states for AA5754 may be due to the lower hardness value of this alloy in comparison with AA5083, which leads to a worse wear behaviour.

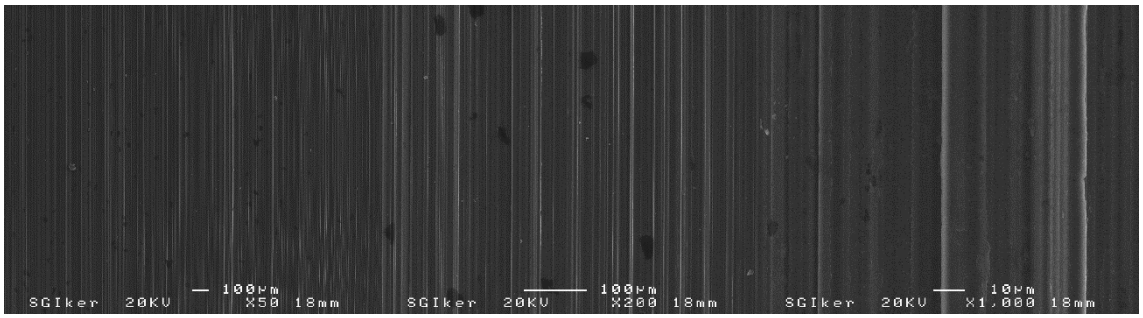


50× 200× 1000×

(**a**)

**Figure 19.** *Cont.*

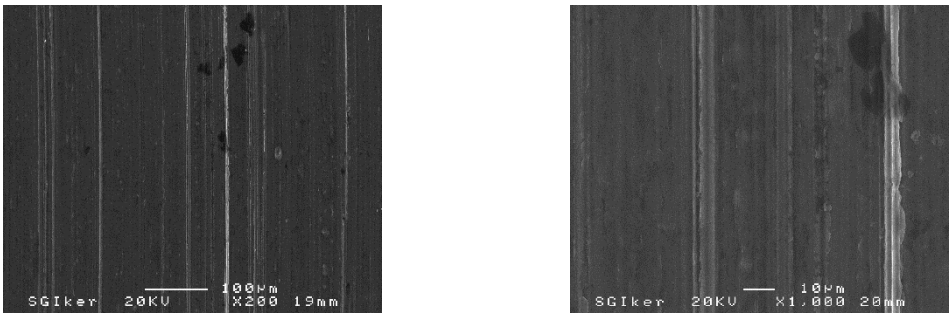


200× 1000×

(**b**)

**Figure 19.** SEM micrographs for AA5754-N0-T380 connecting rod: (**a**) Top zone; (**b**) bottom zone.

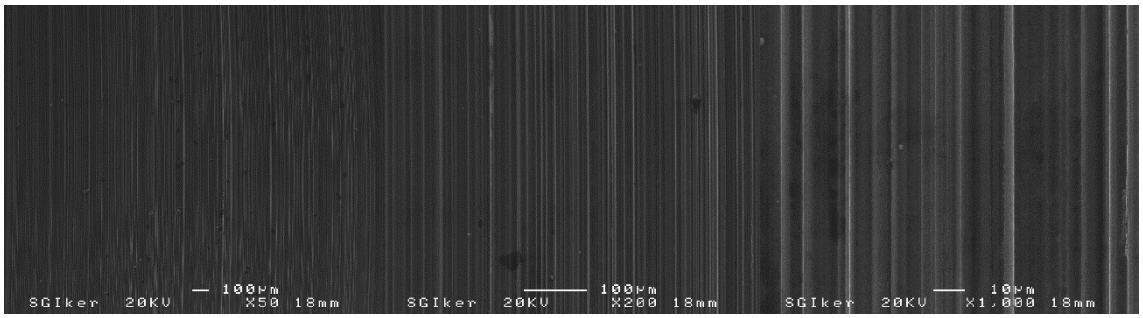


50× 200× 1000×

(**a**)

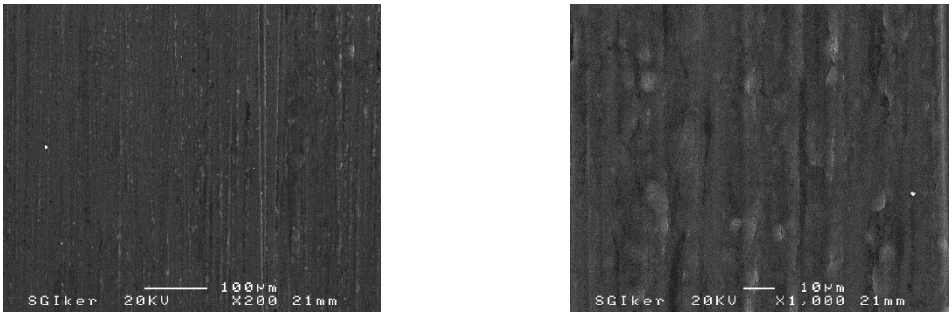


200× 1000×

(**b**)

**Figure 20.** SEM micrographs for AA5754-N2-T150 connecting rod: (**a**) Top zone; (**b**) bottom zone.

## 4. Conclusions

It was found that the connecting rods manufactured from aluminium alloys previously processed by ECAP and after isothermal forging exhibit better in-service wear properties than those isothermally forged from annealed material, at the temperature values under consideration in this study.

The dimensional wear coefficients were determined for the connecting rods made of AA5754 and AA5083 aluminium alloys, by considering two initial states (which were designed as N0 and N2). These mechanical components were manufactured by isothermal forging. From the results attained, it can be affirmed that the connecting rods made of AA5083 and AA5754 aluminium alloys previously

processed by ECAP and isothermally forged at 250 °C and 150 °C, respectively, show an improvement in the in-service wear behaviour.

Moreover, FEM simulations were carried out and a good agreement between both experimental and FEM results was obtained.

**Acknowledgments:** The authors of this present research work acknowledge the support given by the Spanish Ministry of Economy, Industry and Competitiveness (former Spanish Ministry of Economy and Competitiveness) through the Research Project DPI2013-41954-P.

**Author Contributions:** All the authors of this present manuscript have approximately equally contributed to most of the research tasks. However, Carmelo J. Luis and Rodrigo Luri contributed to a great extent to conceive and design the experiments as well as to analyze the data; Juan P. Fuertes, Daniel Salcedo and Javier León contributed to a great extent to perform the experiments; Carmelo J. Luis, Rodrigo Luri and Ignacio Puertas wrote the paper.

**Conflicts of Interest:** The authors declare no conflict of interest.

## References

1. Segal, V.M.; Reznikov, V.I.; Dobryshevshiy, A.E.; Kopylov, V.I. Plastic working of metals by simple shear. *Russ. Metall.* **1981**, *1*, 99–105.
2. Langdon, T.G.; Zhu, Y.T. The fundamentals of nanostructured materials processed by severe plastic deformation. *JOM* **2004**, *56*, 58–63.
3. Furukawa, M.; Horita, Z.; Langdon, T.G. Developing ultrafine grain sizes using severe plastic deformation. *Adv. Eng. Mater.* **2001**, *3*, 121–125. [CrossRef]
4. Valiev, R.Z.; Langdon, T.G. Principles of equal-channel angular pressing as a processing tool for grain refinement. *Prog. Mater. Sci.* **2006**, *51*, 881–981. [CrossRef]
5. Valiev, R.Z.; Islamgaliev, R.K.; Alexandrov, I.V. Bulk nanostructured materials from severe plastic deformation. *Prog. Mater. Sci.* **2000**, *45*, 103–189. [CrossRef]
6. Bian, M.Z.; Li, Y.L.; Mathesh, M.; Abreu, D.; Nam, N.D. Microstructure and texture evolutions and mechanical properties in pure copper by equal-channel angular pressing. *J. Alloy. Compd.* **2013**, *578*, 369–372. [CrossRef]
7. Soliman, M.S.; El-Danaf, E.A.; Almajid, A.A. Enhancement of static and fatigue strength of 1050 Al processed by equal-channel angular pressing using two routes. *Mater. Sci. Eng. A* **2012**, *532*, 120–129. [CrossRef]
8. Raab, G.J.; Valiev, R.Z.; Lowe, T.C.; Zhu, Y.T. Continuous processing of ultrafine grained Al by ECAP-Conform. *Mater. Sci. Eng. A* **2004**, *382*, 30–34. [CrossRef]
9. Rajinikanth, V.; Arora, G.; Narasaiah, N.; Venkateswarlu, K. Effect of repetitive corrugation straightening on Al and Al-0.25 Sc alloy. *Mater. Lett.* **2008**, *62*, 301–304. [CrossRef]
10. Saito, Y.; Utsunomiya, H.; Tsuji, N.; Sakai, T. Novel ultra-high straining process for bulk materials—Development of the accumulative roll-bonding (ARB). *Acta Mater.* **1999**, *47*, 579–583. [CrossRef]
11. Zhilyaev, A.P.; Langdon, T.G. Using high-pressure torsion for metal processing: Fundamentals and applications. *Prog. Mater. Sci.* **2008**, *53*, 893–979. [CrossRef]
12. Frint, S.; Hockauf, M.; Frint, P.; Wagner, M.F.X. Scaling up Segal's principle of equal-channel angular pressing. *Mater. Des.* **2016**, *97*, 502–511. [CrossRef]
13. Horita, Z.; Fujinami, T.; Langdon, T.G. The potential for scaling ECAP: Effect of sample size on grain refinement and mechanical properties. *Mater. Sci. Eng. A* **2001**, *318*, 34–41. [CrossRef]
14. Valiev, R.Z.; Semenova, I.P.; Jakushina, E.; Latysh, V.V.; Rack, H.J.; Lowe, T.C.; Petruželka, J.; Dluhoš, L.; Hrušák, D.; Sochová, J. Nanostructured SPD processed titanium for medical implants. *Mater. Sci. Forum* **2008**, *584*, 49–54. [CrossRef]
15. Luis Pérez, C.J.; Salcedo Pérez, D.; Puertas Arbizu, I. Design and mechanical property analysis of ultrafine grained gears from AA5083 previously processed by equal channel angular pressing and isothermal forging. *Mater. Des.* **2014**, *63*, 126–135. [CrossRef]
16. Salcedo, D.; Luis, C.J.; Puertas, I.; León, J.; Luri, R.; Fuertes, J.P. FEM modelling and experimental analysis of an AA5083 turbine blade from ECAP processed material. *Mater. Manuf. Process.* **2014**, *29*, 434–441. [CrossRef]
17. Höppel, H.W.; Kautz, M.; Xu, C.; Murashkin, M.; Langdon, T.G.; Valiev, R.Z.; Mughrabi, H. An overview: Fatigue behaviour of ultrafine-grained metals and alloys. *Int. J. Fatigue* **2006**, *28*, 1001–1010. [CrossRef]

18. Kulyasova, O.; Islamgaliev, R.; Mingler, B.; Zehetbauer, M. Microstructure and fatigue properties of the ultrafine-grained AM60 magnesium alloy processed by equal-channel angular pressing. *Mater. Sci. Eng. A* **2009**, *503*, 176–180. [CrossRef]
19. Goto, M.; Han, S.Z.; Kitamura, J.; Yakushiji, T.; Ahn, J.H.; Kim, S.S.; Baba, M.; Yamamoto, T.; Lee, J. S-N plots and related phenomena of ultrafine grained copper with different stages of microstructural evolution. *Int. J. Fatigue* **2015**, *73*, 98–109. [CrossRef]
20. Gröber, D.; Georgi, W.; Sieber, M.; Scharf, I.; Hellmig, R.J.; Leidich, E.; Lampke, T.; Mayr, P. The effect of anodising on the fatigue performance of self-tapping aluminium screws. *Int. J. Fatigue* **2015**, *75*, 108–114. [CrossRef]
21. Ortiz-Cuellar, E.; Hernandez-Rodriguez, M.A.L.; García-Sanchez, E. Evaluation of the tribological properties of an Al-Mg-Si alloy processed by severe plastic deformation. *Wear* **2011**, *271*, 1828–1832. [CrossRef]
22. Li, J.; Wongsa-Ngam, J.; Xu, J.; Shan, D.; Guo, B.; Langdon, T.G. Wear resistance of an ultrafine-grained Cu-Zr alloy processed by equal-channel angular pressing. *Wear* **2015**, *326*, 10–19. [CrossRef]
23. Huang, S.J.; Semenov, V.I.; Shuster, L.S.; Lin, P.C. Tribological properties of the low-carbon steels with different micro-structure processed by heat treatment and severe plastic deformation. *Wear* **2011**, *271*, 705–711. [CrossRef]
24. Edalati, K.; Ashida, M.; Horita, Z.; Matsui, T.; Kakato, H. Wear resistance and tribological features of pure aluminum and Al-$Al_2O_3$ composites consolidated by high-pressure torsion. *Wear* **2014**, *310*, 83–89. [CrossRef]
25. Moshkovich, A.; Lapsker, I.; Rapoport, L. Correlation between strengthening and damage of Cu refined by different SPD processing and friction in different lubricant regions. *Wear* **2013**, *305*, 45–50. [CrossRef]
26. Zhilyaev, A.P.; Shakhova, I.; Belyakov, A.; Kaibyshev, R.; Langdon, T.G. Wear resistance and electroconductivity in copper processed by severe plastic deformation. *Wear* **2013**, *305*, 89–99. [CrossRef]
27. Zhilyaev, A.P.; Shakhova, I.; Belyakov, A.; Kaibyshev, R.; Langdon, T.G. Effect of annealing on wear resistance and electroconductivity of copper processed by high-pressure torsion. *J. Mater. Sci.* **2014**, *49*, 2270–2278. [CrossRef]
28. Zhilyaev, A.P.; Morozova, A.; Cabrera, J.M.; Kaibyshev, R.; Langdon, T.G. Wear resistance and electroconductivity in a Cu-0.3Cr-0.5Zr alloy processed by ECAP. *J. Mater. Sci.* **2017**, *52*, 305–313. [CrossRef]
29. Fuertes, J.P.; León, J.; Luis, C.J.; Salcedo, D.; Puertas, I.; Luri, R. Design, optimization, and mechanical property analysis of a submicrometric aluminium alloy connecting rod. *J. Nanomater.* **2015**, *16*, 1–15. [CrossRef]
30. León, J.; Luis, C.J.; Fuertes, J.P.; Puertas, I.; Luri, R.; Salcedo, D. A proposal of a constitutive description for aluminium alloys in both cold and hot working. *Metals* **2016**, *6*, 244. [CrossRef]
31. Luri, R.; Fuertes, J.P.; Luis, C.J.; Salcedo, D.; Puertas, I.; León, J. Experimental modelling of critical damage obtained in Al-Mg and Al-Mn alloys for both annealed state and previously deformed by ECAP. *Mater. Des.* **2016**, *90*, 881–890. [CrossRef]
32. Avilés, R. *Análisis de Fatiga en Máquinas*; Paraninfo: Madrid, Spain, 2005.
33. Stephens, R.I.; Fatemi, A.; Stephens, R.R.; Fuchs, H.O. *Metal Fatigue in Engineering*; John Wiley & Sons: New York, NY, USA, 2001.
34. Semiatin, S.L. *Forming and Forging*; ASM International: Materials Park, OH, USA, 1996.